

Kinetics of Electrically Enhanced Boron Removal From Silicon Using CaO-SiO₂ and CaO-SiO₂-Al₂O₃ Slag



A.D.P. PUTERA, M.S. ISLAM, K.L. AVARMAA, H.T.B.M. PETRUS, G.A. BROOKS, and M.A. RHAMDHANI

An approach in analyzing the kinetics of reacting metallurgical system enhanced by applied electrical potential difference has been proposed. The approach accounted the electrochemical mechanism by combining Fick's first law and Nernst-Planck equation, building upon the approach by Kim *et al.* and extending it to simultaneously solve the key kinetics parameters of boron diffusivity in slag ($D_{(B)}$) and potential difference ($\Delta\phi_s$) across the slag phase. The approach was utilized to examine the kinetics of enhanced boron removal from silicon with CaO-SiO₂ and CaO-SiO₂-Al₂O₃ slags, in the context of silicon recycling and refining. The model was used to describe the mobility of boron in the molten silicon and slag phases, *i.e.*, boron mass transfer coefficient in liquid silicon (k_m), in the slag (k_s), and the diffusivity of boron in slag phase ($D_{(B)}$). The results demonstrated that the new kinetics model fit well with the experimental data with an average coefficient of determination (R^2 value) of 0.91. The k_s and $D_{(B)}$ were calculated to be in the range of 0.9 to 1.3×10^{-6} and 1.1 to $29.2 \times 10^{-9} \text{ m}^2 \text{ s}^{-1}$, respectively. The application of external voltage was observed to reduce B final concentration in the silicon phase by 18 pct from approximately 120 to 100 ppmw in all samples. The addition of Al₂O₃ in the slag phase consistently reduced the mobility of boron in the slag phase by approximately 50 pct.

<https://doi.org/10.1007/s11663-023-02756-x>
© The Author(s) 2023

I. INTRODUCTION

As early as 1839, Edmond Becquerel discovered that electricity can be produced from a chemical battery exposed to the sun,^[1] which is the basis of photovoltaic effect. Photovoltaic (PV) cells are thin devices that convert

solar energy into electricity, which are utilized in many technological applications such as electronics, calculators, telecommunication devices, rooftop panels, and many others. The development and uptake of PV cells have been rising exponentially in recent years. It was reported that in 2020, solar-PV-generated electricity reached 821 TWh globally,^[2] which corresponds to the second-largest growth within the renewable energy sources. From the electricity generation standpoint, solar PV generates 3.1 pct of the global electricity,^[2] of which majority (~90 pct) comes from a polycrystalline silicon-based PV cell. In addition, solar PV is now becoming one of the inexpensive options for electricity generation in many countries, making it more preferable in the coming years.^[2] Modern silicon-based solar PV cell consists of several materials such as glass, aluminum, encapsulating material, cables, silicon wafer, silver (Ag), and trace heavy metals such as lead (Pb) and cadmium (Cd).^[3] In 2030, worldwide solar PV waste production is predicted to reach between 4 and 14 pct of total generation of all electronic waste. This is forecasted to be accompanied by further growth in end-of-life PV cells with an estimated global generation of 78 million tons in 2050.^[4] With these in mind, sustainable recycling and refining methods for silicon to support the growth of the uptake and the management of the associated end-of-life PV cell generated will be vital.

A. D. P. PUTERA is with the Fluid and Process Dynamics (FPD) Group, Department of Mechanical and Product Design Engineering, Swinburne University of Technology, Melbourne, VIC 3122, Australia and also with the Department of Chemical Engineering (Sustainable Mineral Processing Research Group), Faculty of Engineering, Universitas Gadjah Mada, Jl. Grafika No. 2, Yogyakarta 55281, Indonesia. Contact e-mail: aputera@swin.edu.au M. S. ISLAM is with the Department of Nanomaterials and Ceramic Engineering, Bangladesh University of Engineering and Technology, Dhaka 1000, Bangladesh. K. L. AVARMAA, G. A. BROOKS and M. A. RHAMDHANI are with the Fluid and Process Dynamics (FPD) Group, Department of Mechanical and Product Design Engineering, Swinburne University of Technology, Melbourne, VIC, 3122. Contact e-mail: arhamdhani@swin.edu.au H. T. B. M. PETRUS is with the Department of Chemical Engineering (Sustainable Mineral Processing Research Group), Faculty of Engineering, Universitas Gadjah Mada, Jl. Grafika No. 2, Yogyakarta 55281.

Manuscript submitted September 30, 2022; accepted February 24, 2023.

Article published online March 17, 2023.

There are several metallurgical techniques to recycle and refine primary and secondary silicon resources (including those from end-of-life PV cell), which have been summarized in the previous work.^[4] In terms of pyrometallurgical route, the major processes include solvent refining (including slag treatment), directional solidification, vaporization, and electrorefining.^[5,6] Of the many impurities contained in silicon resources, boron (B) and phosphorus (P) are detrimental and difficult to remove. Yuge *et al.* utilized electrons beam to remove phosphorus from Si melt and plasma to remove boron in the next step.^[7] Other investigators used directional solidification process (1273 to 1473 K) to refine silicon from boron impurity which successfully reduced boron concentration from 10 to 0.1 ppm.^[7] A three-layer electrorefining technique has been studied and used to refine MG-grade silicon into pure silicon, down to the 6N purity range using a high-melting-point fluoride electrolyte.^[8] Nevertheless, this technique was reported to be not sufficient to achieve solar grad purity for certain elements, boron being one of them. Islam and Rhamdhani^[9] studied the kinetics of boron removal from silicon using CaO-SiO₂ and CaO-SiO₂-Al₂O₃ slags at 1773 to 1873 K (1500 to 1600 °C) and reported that the removal rate generally stabilized after 120 min and boron was reduced from 300 to around 100 ppm. Another work to enhance the removal of boron and also phosphorus from silicon in the slag treatment was carried out by Thomas *et al.*^[10] through silicon alloying. It was reported in this study that alloying can affect the activity of boron and phosphorus and their removal rate.

A. Electrically Enhanced Metal–Slag Reactions

It has been widely known that high-temperature reactions between molten metal and slag are naturally electrochemical,^[11] which means that they involve the transfer of both matters and electrons. There have been many studies demonstrating the electrochemical aspect of these reactions, which has been summarized in the work of Judge *et al.*^[12] In this work, Judge *et al.* studied and measured the electrochemical properties of molten pure iron/slag reaction at 1873 to 1973 K (1600 to 1700 °C).^[12] The ramification of the electrochemical nature of slag–metal reactions is that the reactions themselves can be manipulated (enhanced or retarded) by applying external current to the system.

Although there have been many studies demonstrating the electrochemical nature of metal–slag reactions, there are only limited studies that investigated the mechanisms and kinetics of electrically enhanced refining in metal–slag systems. Judge *et al.*^[13] investigated the electrochemical reaction of steel decarburization. Although the reaction mechanism was explained thoroughly, the kinetic was not discussed in detail. By utilizing the overall mass transfer coefficient, the study did not distinguish the mass transfer coefficient between slag and metal phase. Lee and Min^[14] studied the desulfurization of Cu metal using electric enhanced slag treatment and found that the sulfur partitioning ratio can be enhanced using the external potential. However,

the study mentioned that the sulfur partitioning ratio was difficult to explain using ideal Nernst equation because there was decrease in the effective potential applied to the electrochemical double layer (IR drop). Using a different approach, Kim and Kang^[15] attempted to correlate electrochemical desulfurization of iron using CaO-Al₂O₃-MgO_{saturated} slag at equilibrium. The study successfully correlates the equilibrium sulfur partitioning ratio using Nernst equation by defining the resistance of the electrochemical system. In addition, they found that slag with lower CaO/Al₂O₃ (C/A) ratio is desirable for the desulfurization. Islam *et al.*^[9,11,16] studied boron removal from silicon to slag and demonstrated that application of voltage difference during the reaction provides an increase in the overall kinetics; as well as the extent of B removal (boron equilibrium distribution). Islam *et al.*^[11] proposed that boron distribution coefficient in the slag and silicon at equilibrium (L_B^0) can be shifted to a new equilibrium value (L_B) when external potential difference across the system is applied and proposed a theoretical correlation (based on Nernst equation) following Eq. [1]:^[11]

$$\Delta E \cong \frac{RT}{3F} \ln \left(\frac{L_B}{L_B^0} \right), \quad [1]$$

$$L_B = \frac{(\text{wt pct } B)}{[\text{wt pct } B]}, \quad [2]$$

where ΔE , R , T , and F are the potential difference (V), the ideal gas constant (8.314 J mol⁻¹ K⁻¹), temperature (K), and the Faraday's constant (96,485 C mol⁻¹). L_B and L_B^0 are the boron distribution coefficient at applied and zero external potential, while (wt pct B) and [wt pct B] are the concentration of boron in the slag and silicon phase, respectively. Based on Eq. [1], Islam *et al.*^[11] calculated that the application of external voltage up to 300 mV in the Si-B melt and CaO-SiO₂-Al₂O₃ slag system increased the boron distribution coefficient (L_B) by a factor of 1.2. This increase of L_B was underpredicted as the actual voltage across the slag was much smaller due to resistance in the system (slag, silicon, and circuit), which was demonstrated from the experimental results. In this study, Islam *et al.*^[11] also carried out limited kinetic analysis utilizing a general mass transfer controlled model and showed that the mass transfer coefficient was increased by a factor of 1.4 with increasing external potential from 0 to 3 V. In a separate study, Islam *et al.*^[16] extended the study by increasing the applied potential to 3.5 V and reported that apparent rate and the boron partition ratio were both increased by a factor of 1.6.

Wang *et al.*^[17] further investigated the boron removal from silicon alloy using 40CaO-40SiO₂-20Al₂O₃ (wt pct) slag at 1773 K (1500 °C) in argon atmosphere for 1 h. They proposed a mechanism in which the reduction of SiO₂ into Si was through a transfer of oxygen in the slag phase to the silicon alloy phase. This is similar to the mechanism proposed by Judge *et al.*,^[13] where oxygen

was supplied by the reduction of silica. In addition, a solid Si deposit was reported to form on the electrode submerged in the slag phase. They proposed that oxygen molecules diffuse towards the silicon phase under an electric field and then react with the boron molecules at the interface of silicon and slag, creating boron oxide ions (BO_3^{3-}) that is transferred back into the slag phase.^[17] No explicit correlations between the applied voltage with the rate of reactions were presented in both Islam *et al.* and Wang *et al.* kinetic studies.

In a different system, Kim *et al.*^[18,19] investigated the electrochemical desulfurization of molten steel by molten slag and proposed a kinetic model using a combination of Fick's first law of diffusion and Nernst–Planck Equation^[19] and explicitly expressed the applied voltage in the kinetic equation. The study showed that the calculated electric potential at the interface in the system increased linearly with increasing external current applied to the system. The study also demonstrated that the rate of the desulfurization was enhanced and final S concentration in steel was lowered with the application of external electric current, but was more efficient at lower temperature.^[19] However, the study assumed that the diffusivity of sulfur in the slag phase did not change at various external potential. The initial sulfur concentration for the external potential treatment was also different from the system with no treatment.

Although there have been a number of studies demonstrating the application of external voltage/current enhanced the removal of impurities in pyrometallurgical refining,^[11,18,20,21] no adequate kinetic models were presented. This means that the addition of electric voltage is not explicitly expressed in the kinetic model, in particular, for the case of boron removal from silicon during enhanced refining by slag. The current work presents a larger kinetic data set of enhanced boron removal from silicon by a $\text{CaO-SiO}_2/\text{CaO-SiO}_2\text{-Al}_2\text{O}_3$ slag system; and also analyses on the kinetics of the reaction by extending the model developed by Kim *et al.*^[18,19] to investigate how the applied voltage affects the mass transfer coefficient and the overall process.

II. EXPERIMENTAL METHODOLOGY

A. Materials

Master slags used in the current study were made in a laboratory using high-purity oxides powder of CaCO_3 (99.95 wt pct), SiO_2 (99.5 wt pct), and Al_2O_3 (99 wt pct), obtained from Alfa Aesar. CaCO_3 was dried at 773 K (500 °C) for 5 h, followed by heating for 2 h at 1523 K (1250 °C) to transform the carbonate to CaO. For each composition of the slag (as presented in Table I), as much as 20 g of powder mixture was weighed and mixed in a ball mill for 48 h. Using a 13-kW Ambrell EkoHeat induction furnace, the master slags were prepared by

melting batches of mixed oxides of appropriate compositions in graphite crucibles. The master slags were melted twice at temperature of 1763 ± 15 K (1490 ± 15 °C) to allow homogenization.

Master silicon alloys were made using high-purity silicon (99.9999 wt pct) and boron (99.9 wt pct) powder, obtained from Alfa Aesar. Silicon and boron powders of appropriate compositions were mixed in a ball mill and melted using a graphite crucible in a 10.3 kW-RHTV 120-300/18 Nabertherm vertical tube furnace in ultra-high-purity argon atmosphere. Ultra-high-purity Ar gas (99.999 pct) was used to ensure an inert atmosphere during the experiment. To ensure homogeneous mixing, the melt was stirred with alumina rod. An initial boron concentration of 375 ppm was selected for the study. ICP-AES analyses were carried out on the master slags and master alloys to confirm their compositions.

B. Details of Experimental Apparatus and Parameters

A schematic of the RHTV 120-300/18 Nabertherm vertical tube furnace setup used in the current study is presented in Figure 1. A DC power supply was connected to apply the external potential difference to the liquid slag–metal system. A computer-based data acquisition card (National Instrument DAQ Card 9250) was used to record the voltage (to maintain the voltage supplied in the system) during the experiments. The DC power supply was connected to the graphite electrodes, veiled by alumina tube to protect from mixed cell contact during immersion.^[22] At first, an alumina crucible filled with mixture of slag and Si alloy was placed on top of an alumina pedestal in the cold zone at room temperature. The furnace was then sealed, and the chamber was evacuated using a rotary pump before backfilled with Ar, and the target temperature of 1823 K (1550 °C) was set. A flow rate of 250 ml min^{-1} was used and controlled using Aalborg Command Module (a microprocessor-driven digital command modules for mass flow controller) during the experiments. After the furnace reached 1823 K (1550 °C), the crucible was positioned into the hot zone by lifting the pedestal. The starting point of the reaction ($t = 0$) was considered as the moment when the crucible was set to this position. The Si-B and slag in the crucible were let to react for different reaction times. When the time of the reaction was reached, the crucible was withdrawn into the cold zone by lowering the pedestal and quenched by flushing Argon gas. The hotzone was 300 mm from the bottom flange and the length of the hotzone was 100 mm.^[22] The crucible system was then collected to retrieve the silicon alloy and slag samples for further characterizations and analyses.

The experimental conditions and parameters investigated in the current work are presented in Table I. The calcium oxide-to-silicon dioxide mass ratio in the slag was maintained at approximately 35:65, and alumina

Table I. Summary of the Parameters and Conditions Investigated in the Current Study

Type of Slag (wt pct)	T, K	Time, Seconds	DC Voltage, V	Slag-to-Silicon Mass Ratio	m_{Si} , kg
35CaO-65SiO ₂	1823	0, 600, 900, 1800, 2700,	0, 2, 3	1.8	0.002
32CaO-59SiO ₂ -9Al ₂ O ₃		3600, 5400, 7200, 10,800	0, 2, 3, 5		
30CaO-55SiO ₂ -16Al ₂ O ₃			0, 2.5, 3.5, 5		

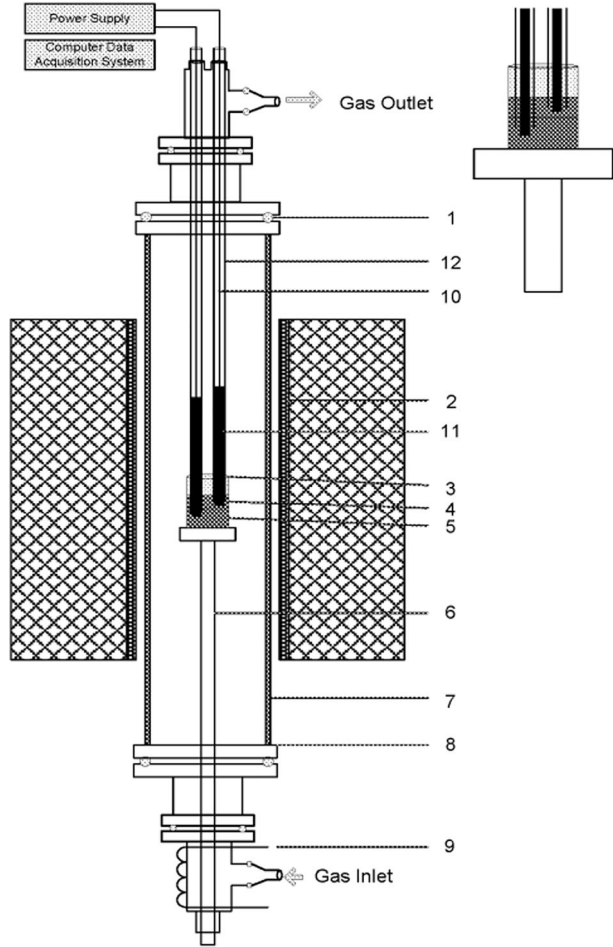


Fig. 1—A schematic of a vertical tube furnace setup for the kinetics experiments. Legend: 1-Silicone O-ring, 2- MoSi₂ heating Element, 3-Crucible, 4-Silicon, 5-Slag, 6-Alumina Pedestal, 7-Alumina Tube, 8-Water cooled flanges, 9-Copper coil, 10-Kanthal wire, 11-Graphite electrode, 12-Electrode cover. Reprinted with permission from—Ref. [16].

concentration was varied at 0, 9 and 16 wt pct. The slag-to-silicon mass ratio was initially set at 1.8 and only one temperature was studied, *i.e.*, 1823 K (1550 °C). The reaction times selected were 10, 15, 30, 45, 60, 90, 120, and 180 min and the applied external voltage was in the range from 0 to 5 V.

C. Details of Characterization Techniques

The boron concentration in the collected samples was analyzed using a Varian 730ES inductively coupled plasma atomic emission spectroscopy (ICP-AES). Samples were prepared by physically separating solid slag

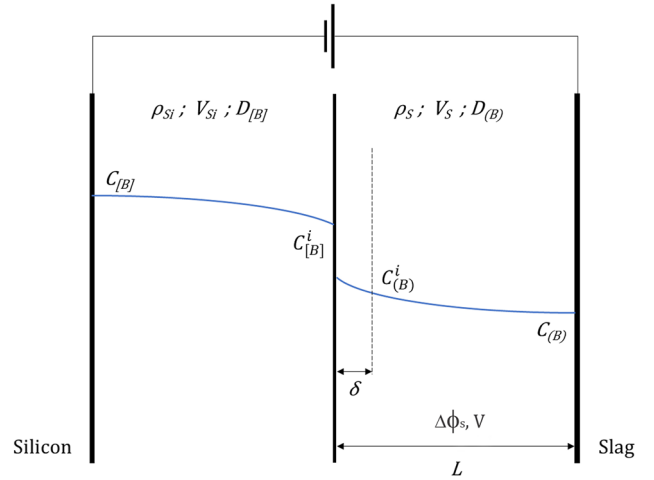


Fig. 2—Schematic diagram of boron concentration in liquid silicon and molten slag.

and silicon phases after cooling. Slag and silicon samples were crushed and grounded separately to powder samples for analysis. For silicon, the samples were fused with sodium peroxide (Na₂O₂) solution and dissolved in acid solution. ICP-AES was able to analyze the boron concentration and other elements such as calcium, aluminum, and phosphorus in the silicon and slag samples. The analyses were conducted at Spectrometer Services Pty Ltd, Coburg, Melbourne.

III. RESULTS AND DISCUSSION

A. Kinetics Analysis Approach

The kinetic model from Kim *et al.*^[16] was utilized and further extended in the current study. Let us consider a liquid silicon and molten slag two-phase system as illustrated in Figure 2. In the silicon phase, the mass flux of boron, B, can be expressed based on the Fick's first law of diffusion as^[19,23]

$$J_{[B]} = -\frac{dC_{[B]}}{dt} = D_{[B]} \frac{\partial C_{[B]}}{\partial x}, \quad [3]$$

$$-D_{[B]} \frac{\partial C_{[B]}}{\partial x} \approx k_m (C_{[B]} - C_{[B]}^i), \quad [4]$$

where $J_{[B]}$, $D_{[B]}$, $C_{[B]}$, k_m , and $C_{[B]}^i$ are the flux of B (mol m⁻² s⁻¹), the diffusivity of B in liquid silicon (m² s⁻¹), the molar concentration of B in the bulk silicon (mol m⁻³), the mass transfer coefficient of B in the

liquid silicon (m s^{-1}), and the molar concentration of B at the interface (mol m^{-3}), respectively. In the slag phase, by considering the Fick's first law Eq. [4], the Nernst–Planck equation,^[24] and with the application of potential difference across the slag, one can derive the following correlation:

$$C_{[B]}^i = \frac{C_{[B]}\delta k_m + C_{(B)}D_{(B)}\left(1 - \frac{Fz}{RT} \frac{\delta}{L} \Delta\phi_s\right)}{\delta k_m + L_B^0 D_{(B)} \exp\left(\frac{Fz}{RT} \Delta\phi_s\right)}, \quad [5]$$

where δ , $C_{(B)}$, $D_{(B)}$, F , z , R , T , $\Delta\phi_s$ and L_B^0 , represent the interface layer thickness (m), the concentration of boron in slag (mol m^{-3}), diffusivity of boron in the slag phase ($\text{m}^2 \text{s}^{-1}$), Faraday's constant (C mol^{-1}), electric charge of boron (3),^[11] ideal gas constant ($8.314 \text{ J mol}^{-1} \text{ K}^{-1}$), the prevailing temperature (K), internal electric potential difference across the slag phase (V), and the distribution coefficient of boron without applied electric potential, respectively. The data input is provided in Table VII in the Appendix section. A more detailed derivation of this equation can be found in Appendix I. It should be noted that in the slag phase, boron existed in the form of (BO_3^{3-}) ion and the corresponding parameters represent this species. From the mass conservation of boron in the system, the concentration of boron in the slag can be expressed as

$$C_{(B)} = (C_{[B]}^0 - C_{[B]}) \frac{V_{\text{Si}}}{V_S}, \quad [6]$$

where V_{Si} and V_S are the volume of silicon phase and slag phase (m^{-3}), respectively. The volume of the slag was calculated by considering the initial mass of the slag and the density of the slag obtained from the work of Muhmood and Seetharaman.^[25] Substituting Eqs. [5] and [6] into Eq. [4], we get

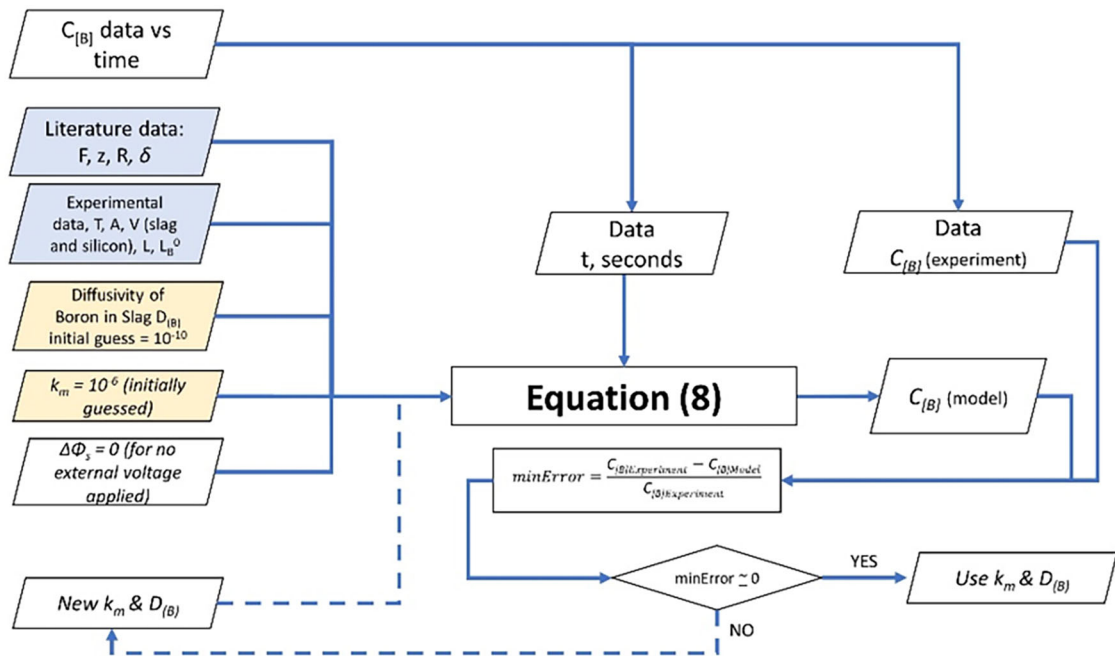
$$\frac{dC_{[B]}}{dt} = -k_m \frac{A D_{(B)} \left(C_{[B]} \left\{ L_B^0 \exp\left(\frac{Fz}{RT} \Delta\phi_s\right) + \frac{V_{\text{Si}}}{V_S} \left(1 - \frac{Fz}{RT} \frac{\delta}{L} \Delta\phi_s\right) \right\} - C_{[B]}^0 \frac{V_{\text{Si}}}{V_S} \left(1 - \frac{Fz}{RT} \frac{\delta}{L} \Delta\phi_s\right) \right)}{\delta k_m + L_B^0 D_{(B)} \exp\left(\frac{Fz}{RT} \Delta\phi_s\right)}. \quad [7]$$

An integration of the above equation was then carried out by assuming a constant $\Delta\phi_s$ with time. The actual value of $\Delta\phi_s$ may change with time. However, it was expected that the change was not significant^[15] like in the case of the current study. The assumption of the $\Delta\phi_s$ to be constant was also an approach taken in the previous study.^[19] Therefore, in the context of the current study, the $\Delta\phi_s$, $D_{(B)}$ and k_s will vary with different system's initial conditions, but they are assumed to be not changing with time during the course of the reaction. Thus, the correlation between $C_{[B]}$ and time (second) can be written as

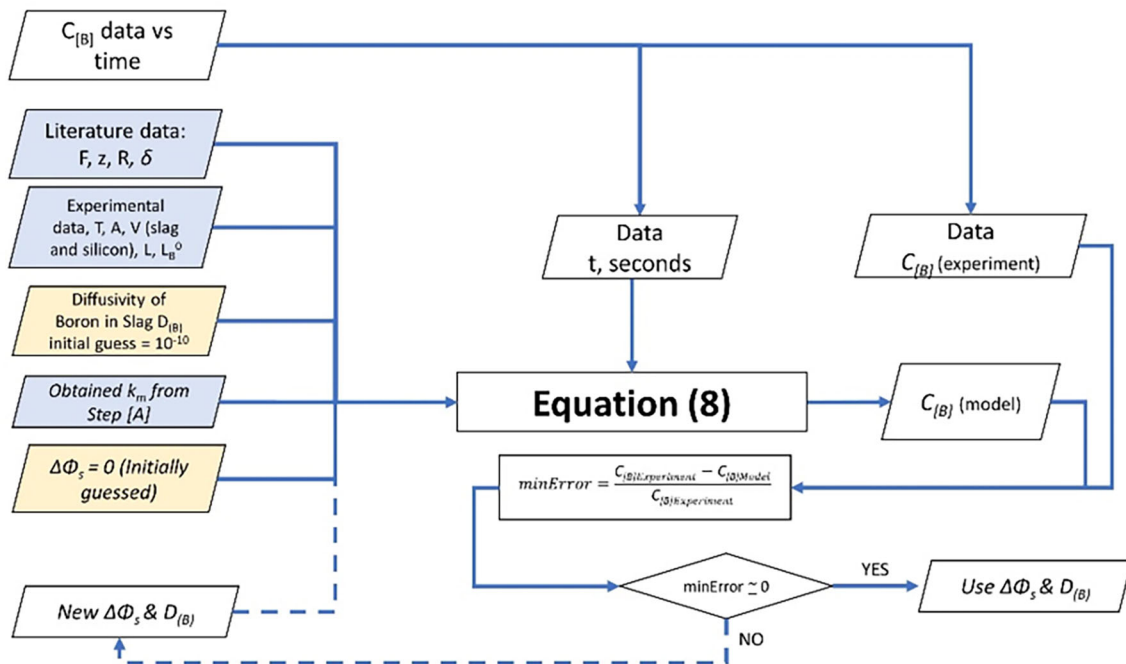
$$C_{[B]} = \frac{C_{[B]}^0 \left\{ L_B^0 \exp\left(\frac{Fz}{RT} \Delta\phi_s\right) \right\} \exp\left(-k_m \frac{A}{V} \frac{\left\{ L_B^0 \exp\left(\frac{Fz}{RT} \Delta\phi_s\right) + \frac{V_{\text{Si}}}{V_S} \left(1 - \frac{Fz}{RT} \frac{\delta}{L} \Delta\phi_s\right) \right\} D_{(B)} t}{\left\{ \delta k_m + L_B^0 D_{(B)} \exp\left(\frac{Fz}{RT} \Delta\phi_s\right) \right\}}\right) + C_{[B]}^0 \frac{V_{\text{Si}}}{V_S} \left(1 - \frac{Fz}{RT} \frac{\delta}{L} \Delta\phi_s\right)}{\left\{ L_B^0 \exp\left(\frac{Fz}{RT} \Delta\phi_s\right) + \frac{V_{\text{Si}}}{V_S} \left(1 - \frac{Fz}{RT} \frac{\delta}{L} \Delta\phi_s\right) \right\}}. \quad [8]$$

The mathematical calculation framework used in this study is shown in Figure 3. Initially, Eq. [8] was fitted with the experimental data for $\Delta\phi_s = 0 \text{ V}$ for the iteration and solving of k_m and $D_{(B)}$ values simultaneously, see Figure 3(a). The obtained k_m was then assumed to be constant for the rest of the data fitting process as the experiments were carried out at isothermal conditions. Utilizing this value of k_m , the values of $D_{(B)}$ and $\Delta\phi_s$ were then solved simultaneously for the case of system with applied external potential considering the experimental data, see Figure 3(b). This is the key difference of the approach utilized in the current study compared to that of from Kim *et al.*^[19] In the study, they assumed the value of $D_{(S)}$ to be constant with various applied potential. This assumption also led to a constant mass transfer coefficient in the slag phase (k_s), as the model was also assuming a constant interface thickness of 10^{-4} m (note that the model was based on a boundary layer/two films diffusion model). In a system with applied external potential, it can be expected that the presence of the potential field in the slag would affect the diffusion of ionic species (such as BO_3^{3-} in the current Si slag system studied) hence also affect the mass transfer coefficient of B in the slag. In the current study, we assumed $\Delta\phi_s$, $D_{(B)}$, and k_s to vary for different initial conditions of the system (temperature, slag composition, initial B concentration, and external applied voltage $\Delta\phi$) but not with time during one set of kinetic experiments. These variables then were solved simultaneously using the kinetic model. In actual transient system, these variables may very likely be changing with time. However, it was assumed that the change was small especially for the system with constant applied external voltage; and rather we were calculating their “average” values over the course of the reaction period using the model.

It should be noted from Eq. [8] that the value of $D_{(B)}$ is determined for the initial reaction rate of the system; meanwhile $\Delta\phi_s$ is determined at the end of the reaction when system has reached equilibrium. From the experimental data, it was observed that the initial decrease of the B concentration occurred within approximately 30 min (1800s) of the reaction, hence only data within this time range were used for the data fitting process to yield $D_{(B)}$. While for $\Delta\phi_s$, the data of the whole time range were used, *i.e.*, until the B concentration reached a plateau, which indicated that the system was at or very close to equilibrium ($\sim 3 \text{ h} = 10,800 \text{ s}$). For the calculation, the interface thickness layer δ was assumed to be



A



B

Fig. 3—The mathematical framework of the model data fitting (A) for the initial sample with 0 V applied, and (B) for samples with applied external potential.

Table II. Summary of experimental data, the concentration of boron in the Si phase at different times of reaction, with various slag types and external voltages—Ref. 22

Time, Seconds	$C_{[B]}$, mol m ⁻³											
	Slag: 35CaO-65SiO ₂			32CaO-59SiO ₂ -9Al ₂ O ₃				30CaO-55SiO ₂ -16Al ₂ O ₃				
	0 V	2 V	3 V	0 V	2 V	3 V	5 V	0 V	2.5 V	3.5 V	5 V	
0	85.7	85.7	85.7	85.7	85.7	85.7	85.7	85.7*	85.7	85.7*	85.7	
600	58.4	57.9	57.4	55.6	52.1	52.1	44.0	55.6	52.1	49.8	46.3	
900	47.5	44.0	44.0	49.2	41.7	41.2	39.4	49.2*	45.2*	41.7*	38.2	
1800	40.5	38.2	35.9	42.2	39.4	35.9	34.7	42.2	39.4	37.1	-	
2700	39.4	34.3	30.1	39.4	34.3	30.1	27.8	39.4	35.9	31.3	27.8	
3600	37.1	31.3	28.9	35.9	32.4	27.8	25.5	35.9*	30.8*	30.1*	25.5	
5400	34.7	29.6	27.8	33.6	30.1	26.6	23.2	33.6	27.8	25.5	-	
7200	32.4	28.9	25.5	30.1	28.9	25.5	20.8	30.1	25.5	20.9	18.5	
10,800	32.4	28.9	25.5	26.6	26.2	25.5	18.5	26.6*	22.0*	19.7*	17.4	

*Selected data have been published in Islam *et al.*^[16]

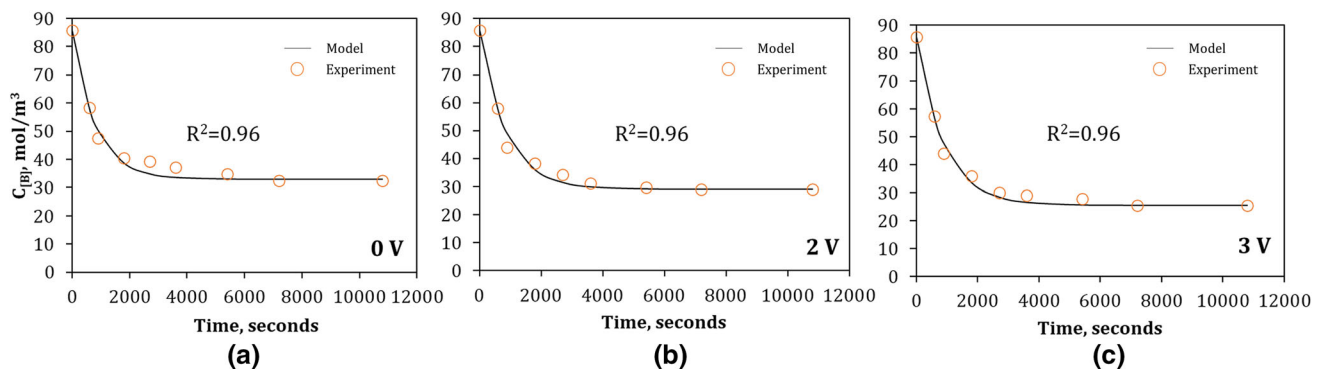


Fig. 4—Variation of boron (B) concentration in silicon phase with time for Si-B alloy and CaO-SiO₂ slag reaction system at 1823 K when (a) 0 V, (b) 2 V, and (c) 3 V external potential were applied.

constant and taken to be 10^{-4} m (100 μ m), similar value taken by Kim *et al.*^[19] The exact interface thickness was not practical nor easy to be measured, and it may change with reaction time. This, however, would be very small compared to the whole system. The full list of the parameters and their values used in the calculations is presented in Appendix II.

Table II presents the boron concentrations calculated from the experimental data generated in the doctoral thesis by Islam at Swinburne University of Technology.^[22] The reported boron concentration in silicon phase in ppmw was converted to mol m⁻³ with the following equations:

$$C_{[B]} = \frac{[\text{percent}B]\rho_{\text{Si}}}{1000M_B}, \quad [9]$$

$$\rho_{\text{Si}} = 2.54 - 2.19 \times 10^{-5}T - 1.21 \times 10^{-8}T^2, \quad [10]$$

where [percentB], M_B , and ρ_{Si} are the concentration of boron in ppmw, atomic mass of boron (10.81 g mol⁻¹), and the density of silicon in kg m⁻³, respectively. The density of liquid silicon, as a function of temperature^[26] is expressed in Eq. [10] and the

resulting $C_{[B]}$ versus time for every studied parameter are presented in Table II. It should be noted that only the selected few data (marked by asterisk *) presented in Table II have been published before by Islam *et al.*^[16]

The resulted $D_{(B)}$ and $\Delta\phi_s$ from the data fitting using the kinetic model are summarized in Table III. The comparisons of the model with the experimental data of B concentration are shown in Figures 4, 5, and 6, for different slag compositions and applied potential. It can be seen from the Figures that the kinetic model fits well with the experimental data with an average R^2 of 0.91. The mass transfer coefficient of boron in the liquid silicon phase (k_m) was calculated to be 6.17×10^{-6} m s⁻¹, which is comparable to the previous studies.^[9,16] Islam *et al.* calculated and compared the mass transfer coefficient in both silicon and slag phases at 1823 K. Although it was concluded in the study that the controlling step was the mass transfer in the slag phase, the mass transfer coefficients in the silicon phase (k_m) were found to be in the range of 1.38 to 2.59×10^{-6} m s⁻¹.^[9] In the case of steel-slag system, Kim *et al.* reported the mass transfer coefficient of sulfur in steel (k_m) varies between 2.25 and 2.80×10^{-6} m s⁻¹ based on their experimental results.^[19]

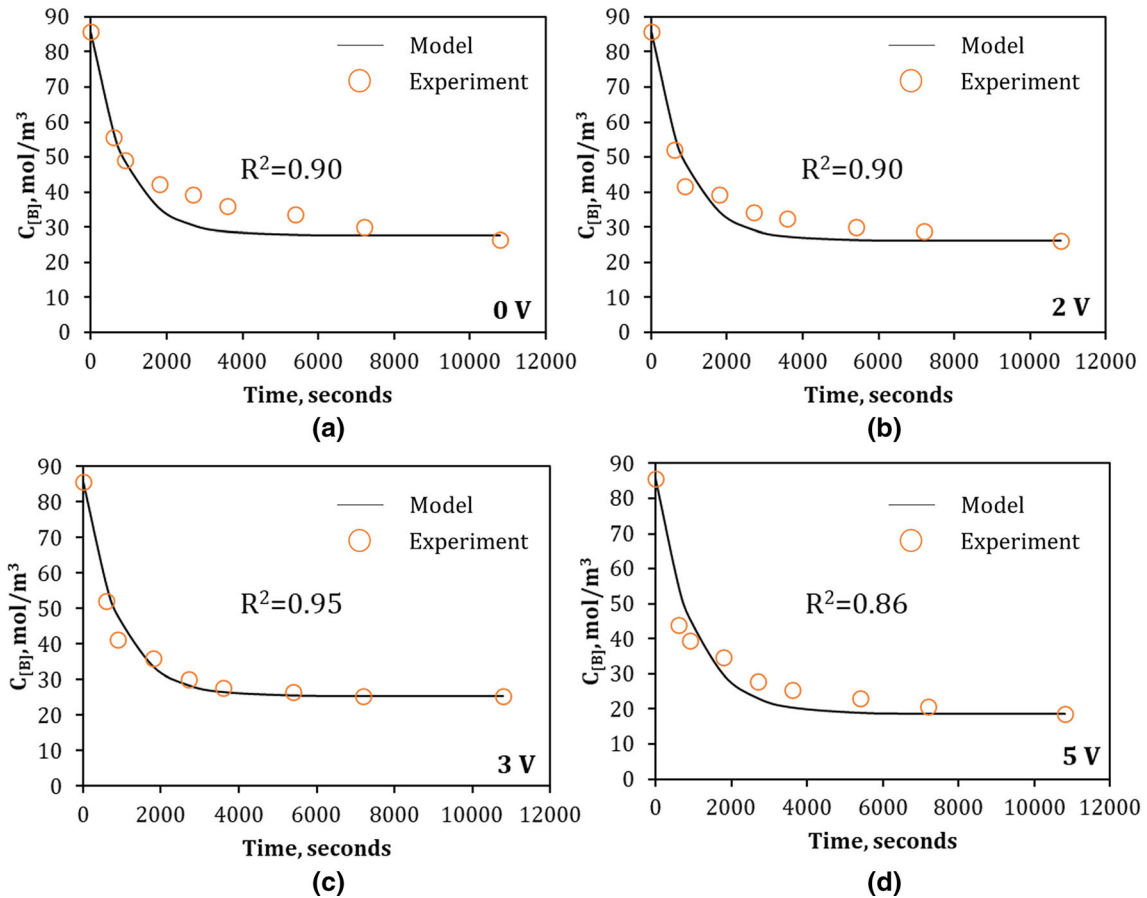


Fig. 5—Variation of boron (B) concentration in silicon phase with time for Si-B alloy and CaO-SiO₂-9 pct Al₂O₃ slag reaction system at 1823 K when (a) 0 V, (b) 2 V, (c) 3 V, and (d) 5 V external potential were applied.

The calculated diffusivity of boron in the slag phase $D_{(B)}$ was found to be in the range of 1.12×10^{-9} to $2.92 \times 10^{-8} \text{ m}^2 \text{ s}^{-1}$. These values are also within the range of boron diffusivity reported in the previous studies.^[18,27,28] Chen *et al.* reported the value of $D_{(B)}$ of $5.24 \times 10^{-9} \text{ m}^2 \text{ s}^{-1}$ in 37CaO-63SiO₂ slag (wt pct) and $8.46 \times 10^{-9} \text{ m}^2 \text{ s}^{-1}$ in 20CaO-17SiO₂-63CaCl₂ slag (weight percent), both at temperature of 1723 K.^[27] For a different element, Kim *et al.* obtained the diffusivity of sulfur in CaO-MgO-SiO₂-Al₂O₃ slag being between 3.95 and $4.69 \times 10^{-10} \text{ m}^2 \text{ s}^{-1}$.^[19]

The results from this study also show that the addition Al₂O₃ in the slag appeared to generally decrease the overall mobility of boron in the slag phase (see the averaged boron diffusivity in Table III). This phenomenon was most likely to be contributed by the effect of Al₂O₃ on the slag viscosity and on the structure of the slag. Although the CaO/SiO₂ ratio in the slag was

aimed to kept constant at approximately 0.54, the addition of alumina could result in the increase of the viscosity of the slag.^[29] The viscosity of the slag with 0, 9, and 16 wt pct of alumina were 1.699, 2.118, and 2.475 P^[22] at 1823 K, respectively (calculated using FactSage software with FToxid solution database). The current study shows that adding 9 pct Al₂O₃ into the slag appeared to decrease the diffusivity of boron in the slag by around 50 pct, and this was also observed for those cases when external potential was applied. Furthermore, the boron diffusivity was observed to further decline by 50 pct in the case of 16 pct Al₂O₃ in the slag. This finding is in line with the previous observation by Islam *et al.*,^[9] which argued that the addition of Al₂O₃ increased the viscosity of the slag hindering the molecule mobilities in the slag phase. Other studies on desulfurization also showed similar results and reported that slag with lower Al₂O₃ with low viscosity would be beneficial from

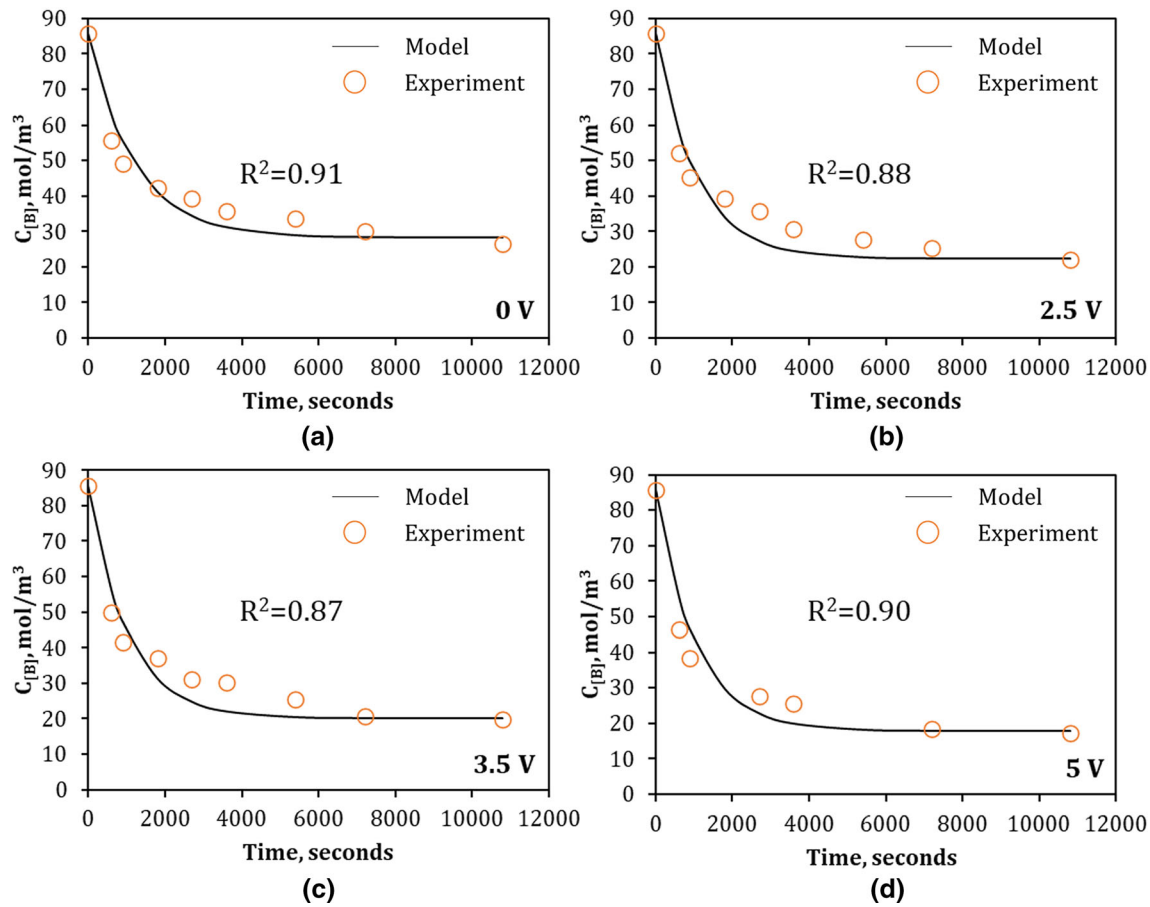
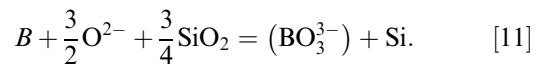


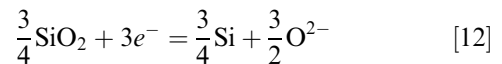
Fig. 6—Variation of boron (B) concentration in silicon phase with time for Si-B alloy and CaO-SiO₂-16 Al₂O₃ slag reaction system at 1823 K when (a) 0 V, (b) 2.5 V, (c) 3.5 V, and (d) 5 V external potential were applied.

operational perspective, and would be a better refining agent.^[30,31] The addition of Al₂O₃ into the basic slag was reported to form [AlO₄]-tetrahedra which behave as a network former, making the microstructure of the slag more viscous and rigid,^[32] hence may reduce the diffusivity of boron.

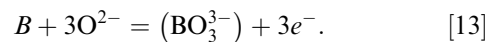
On the other hand, there was a clear trend showing that as the applied potential between the silicon and slag system increased, the final boron concentration in the silicon phase is decreased and the reaction rate was faster. This result is in line with the Le Chatelier's principle, which concludes that a change in one of the variables that describe a system at equilibrium, produces a new shift in the position of the equilibrium that counteracts the effect of this change. As illustrated in Figure 1 before, there are two electrodes immersed in the two molten phases: (1) the slag phase and (2) the silicon phase. The liquid silicon acts as an anode and the liquid slag acts as the cathode. The chemical reactions for the boron removal are^[11]



In the cathode, the reaction is



In the anode, the reaction is



Referring to Figure 2, the DC power supply was set to transfer electrons to the liquid slag phase and taking away electrons from the liquid silicon phase. Based on reaction 12, the electron supply would increase the amount of silica reacted and thus, producing more oxygen. The oxygen molecules are then transferred to the silicon phase to react with the boron,^[17] as shown in reaction 13. Conversely, shifting the direction of the DC power supply will result in less boron consumed. Although this shifting was not carried out in this

Table III. Parameter Results (k_m , $D_{(B)}$, and $\Delta\phi_s$) from Data Fitting to Kinetic Model

Slag Type (Weight Percent)	Viscosity, P	Applied Voltage, V	k_m , m s ⁻¹	Parameter Results		
				$D_{(B)}$, m ² s ⁻¹	$\Delta\phi_s$, V	
35CaO-65SiO ₂	1.699*	0	6.17×10^{-6}	1.23×10^{-8}	2.00×10^{-8} (average)	0
		2		1.85×10^{-8}		0.0107
		3		2.92×10^{-8}	0.0205	
32CaO-59SiO ₂ -9Al ₂ O ₃	2.118*	0		8.19×10^{-9}	1.29×10^{-8} (average)	0
		2		1.18×10^{-8}		0.0047
		3		1.48×10^{-8}	0.0067	
		5		1.70×10^{-8}	0.0291	
30CaO-54SiO ₂ -16Al ₂ O ₃	2.475*	0		1.12×10^{-9}	3.70×10^{-9} (average)	0
		2.5		2.42×10^{-9}		0.0174
		3.5		4.38×10^{-9}	0.0250	
		5		6.87×10^{-9}	0.0334	

*Calculated using FactSage utilizing FToxid solution database.

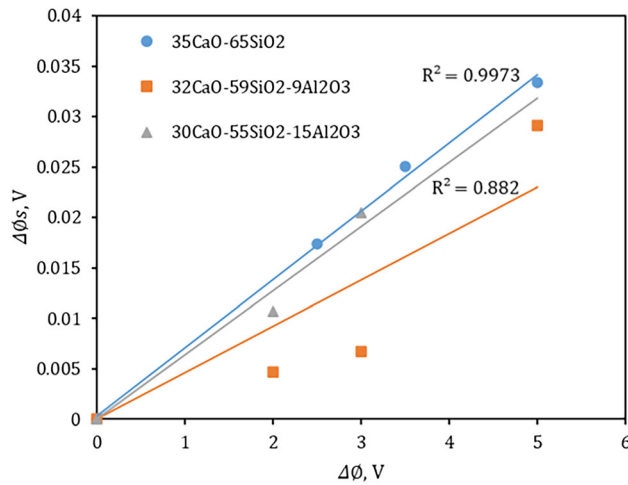


Fig. 7—Calculated potential difference across the slag phase ($\Delta\phi_s$) as a function of the applied potential ($\Delta\phi$) to the system for different types of CaO-SiO₂-Al₂O₃ slags at 1823 K.

research, the phenomenon was demonstrated by Kim *et al.*^[19] In addition, by enhancing the equilibrium condition, greater driving force in the kinetic reaction existed in the reaction (mathematically explained by L_B variable in Eq. [8]). Therefore, the reaction rate was also enhanced.

Table III also shows that the instantaneous boron diffusivity consistently increased with increasing applied potential. This result demonstrated that applying external potential both enhanced the reaction rate and reduced the equilibrium boron concentration in silicon.

The electrical potential difference ($\Delta\phi_s$) across the slag phase that resulted from the applied external potential ($\Delta\phi$) to the system has been calculated using Eq. [8], and the results are plotted in Figure 7. As mentioned by Lee and Min,^[14] there will be differences between the applied potential and the actual potential in the system. The figure indicates that the correlation between the

Table IV. Obtained Mass Transfer Coefficient (k_s^o) with Different Applied Potentials ($\Delta\phi$) for Different Types of CaO-SiO₂-Al₂O₃ Slags at 1823 K

Sample (Weight Percent)	$\Delta\phi$, V	* k_s , m s ⁻¹
35CaO-65SiO ₂	0	2.59×10^{-6}
	2	3.59×10^{-6}
	3	4.25×10^{-6}
32CaO-59SiO ₂ -9Al ₂ O ₃	0	1.86×10^{-6}
	2	2.36×10^{-6}
	3	2.76×10^{-6}
	5	3.29×10^{-6}
30CaO-54SiO ₂ -16Al ₂ O ₃	0	1.38×10^{-6}
	2.5	1.62×10^{-6}
	3.5	1.86×10^{-6}
	5	2.53×10^{-6}

*Islam *et al.*^[9,16,22]

calculated $\Delta\phi_s$ and the applied external potential appeared to vary quite linearly (except the data point at 9 pct Al₂O₃ for 5 V). It can be seen from Figure 7 that the effect of alumina on the $\Delta\phi_s$ is quite complex. The $\Delta\phi_s$ was decreasing with the increase in Al₂O₃ concentration up to 9 wt pct, but then increased again with further increase of Al₂O₃ to 16 wt pct. It is not clear at the moment (with the limited data available) the reason for this trend. This may be related to the amphoteric effect of the Al₂O₃ on the conductivity of the slag. Further study correlating the structure of the slags with their conductivity will be needed to clearly explain the effect of Al₂O₃ addition. In general, it has been reported that the presence of Al₂O₃ generally decreases the electrical conductivity of slag.^[33] Zhang *et al.* reported that for CaO-SiO₂-Al₂O₃ slag at 1823 K and CO/CO₂ = 0.2 atmosphere, increasing the ratio of CaO/Al₂O₃ has two effects: (1) decreasing the total electricity conductivity insignificantly at C/A ratio between 0.5 and 1.25 and (2) increasing the total electricity conductivity at C/A ratio beyond 1.25.^[34]

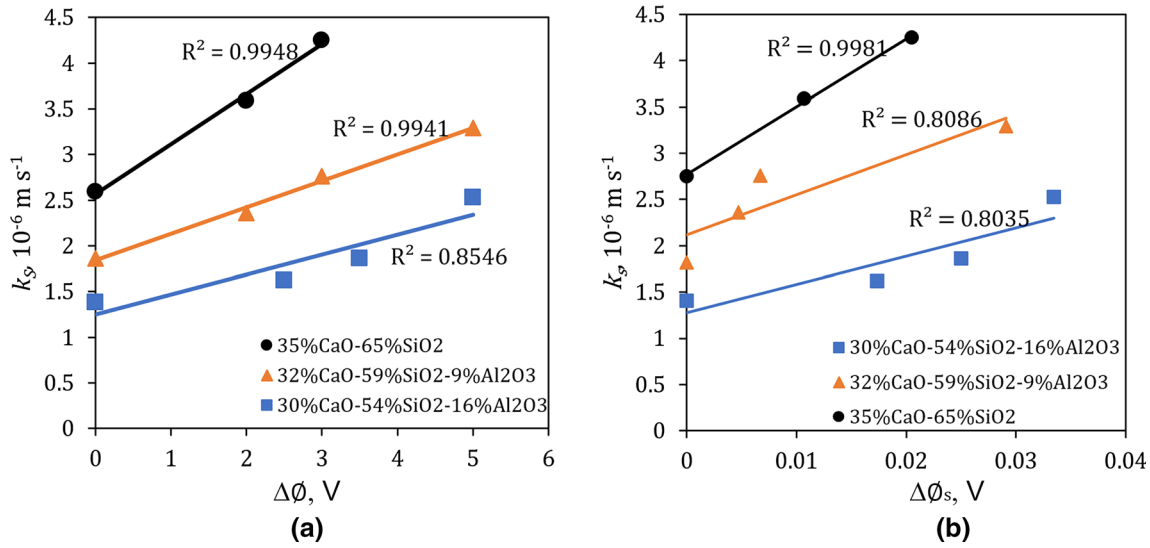


Fig. 8—Variation of the slag-phase mass transfer coefficient (k_s) calculated using slag mass transfer controlled kinetic model with (a) applied external potential difference ($\Delta\phi$) from Islam *et al.*, and (b) calculated potential difference across the slag ($\Delta\phi_s$); for the different types of CaO-SiO₂-Al₂O₃ slags.

Table V. Predicted Mass Transfer Coefficient (k_s) with Different Potential Across the Slag ($\Delta\phi_s$) and Boron Diffusivity in the Slag ($D_{(B)}$)

Sample (Weight Percent)	$D_{(B)}$, m ² s ⁻¹	$\Delta\phi_s$, V	k_s , m s ⁻¹
35CaO-65SiO ₂	1.23×10^{-8}	0	1.25×10^{-6}
	1.85×10^{-8}	0.0107	1.28×10^{-6}
	2.92×10^{-8}	0.0205	1.30×10^{-6}
32CaO-59SiO ₂ -9Al ₂ O ₃	8.19×10^{-9}	0	1.24×10^{-6}
	1.18×10^{-8}	0.0047	1.27×10^{-6}
	1.48×10^{-8}	0.0067	1.28×10^{-6}
30CaO-54SiO ₂ -16Al ₂ O ₃	1.70×10^{-8}	0.0291	1.29×10^{-6}
	1.12×10^{-9}	0	0.91×10^{-6}
	2.42×10^{-9}	0.0174	1.15×10^{-6}
	4.38×10^{-9}	0.0250	1.23×10^{-6}
	6.87×10^{-9}	0.0334	1.27×10^{-6}

B. Correlation Between k_s and $\Delta\phi_s$

In the previous studies, Islam *et al.*^[9,16,22] carried out a kinetic analysis of the system and reported that the reaction was controlled by mass transfer of boron in the slag phase. In these studies, they utilized a slag mass transfer-controlled kinetic model as shown in Eq. [14]:

$$\frac{V_{Si}}{A} \cdot \frac{C_{[B]}^e}{C_{[B]}^0 + C_{(B)}^0} \cdot \ln\left(\frac{C_{[B]} - C_{[B]}^e}{C_{[B]}^0 - C_{[B]}^e}\right) = -k_s \cdot t, \quad [14]$$

where k_s is the mass transfer coefficient of B in the slag. Using Eq. [14], k_s was calculated from the data for the different conditions, and the results are presented in Table IV and Figure 8(a).

One can develop a plot to evaluate how k_s varies with the $\Delta\phi_s$ (calculated potential difference across the slag phase; calculated in Section III—A). The variation of

the calculated potential ($\Delta\phi_s$) across the slag phase and slag-phase mass transfer coefficient (k_s) is presented in Figure 8(b). Similar to Figure 8(a), the plot shows that the mass transfer coefficient in slag, which determines the overall reaction rate, increased with increasing potential difference across the slag. In addition, the increase of Al₂O₃ in the slag phase appeared to also decrease the k_s , which is consistent to the trend observed in Table III.

The slag mass transfer-controlled kinetic model utilized by Islam *et al.*^[9] did not provide a correlation between the potential difference and k_s (nor the boron concentration in silicon). In the current study, we attempt to correlate k_s with $\Delta\phi_s$. Let us begin with Eq. (7) which explains the transfer rate of boron concentration in silicon phase and the conventional mass transfer rate from the previous research^[9,35]:

$$\frac{dC_{[B]}}{dt} = \frac{Ak_s}{V_{Si}} \left(\frac{C_{[B]0}}{C_{[B]e}} \left((C_{[B]} - C_{[B]e}) \right) \right). \quad [15]$$

As the above two equations have to be equal, we can input Eq. [16] into Eq. [7], and solve k_s with a final expression as the following (see Appendix III for detailed derivation):

$$k_s = \frac{k_m C_{[B]e} D_{(B)} (L_B^0 \exp(\frac{Fz}{RT} \Delta\phi_s))}{(C_{[B]0} - C_{[B]e}) \{ \delta k_m + L_B^0 D_{(B)} \exp(\frac{Fz}{RT} \Delta\phi_s) \}}. \quad [16]$$

Equations [7] and [8] can be combined and rearranged into an integrated logarithmic kinetic equation form as shown in Eq. [17].

$$Y \ln Z = -k_s t, \quad [17]$$

where

$$Y = \frac{C_{[B]e} (L_B^0 \exp(\frac{Fz}{RT} \Delta\phi_s)) V_{Si}}{\left\{ L_B^0 \exp(\frac{Fz}{RT} \Delta\phi_s) + \frac{V_{Si}}{V_s} (1 - \frac{Fz}{RTL} \Delta\phi_s) \right\} (C_{[B]0} - C_{[B]e}) A} \quad [18]$$

$$Z = \frac{C_{[B]} \left\{ L_B^0 \exp(\frac{Fz}{RT} \Delta\phi_s) + \frac{V_{Si}}{V_s} (1 - \frac{Fz}{RTL} \Delta\phi_s) \right\} - C_{[B]}^0 \frac{V_{Si}}{V_s} (1 - \frac{Fz}{RTL} \Delta\phi_s)}{C_{[B]}^0 \left\{ L_B^0 \exp(\frac{Fz}{RT} \Delta\phi_s) \right\}} \quad [19]$$

Equation [15] can now be used to predict the k_s from the obtained $D_{(B)}$ and $\Delta\phi_s$ presented in Table III and the results are shown in Table V.

As shown in Table V, the calculated mass transfer coefficients in the slag (between 1 and $1.3 \times 10^{-6} \text{ m s}^{-1}$) appeared to be lower compared to those determined using the general mass transfer kinetic model (Eq. [11] and Table IV). Nevertheless, they were in the same order and the trend was quite similar.

Equations [8], [16], and [17] were also applied to other data published by Wang *et al.*^[17] which studied the refining of Si-B alloy (300 ppm) with 40CaO-40-SiO₂-20Al₂O₃ (weight percent) slag at 1773 K and 1

atmosphere using 3 V external potential. In this study, they utilized a mass ratio of slag to silicon of 5 and carried out the experiment in an argon atmosphere. Their data were fitted using the two approaches: (1) the conventional method of Eq. [11], and (2) the newly developed models, *i.e.*, Equations [8], [16], and [17]. The results are presented in Table VI and Fig. 9.

It can be seen from Table VI that the conventional mass transfer kinetics model (Eq. 14) resulted in the value of k_s of $5.58 \times 10^{-6} \text{ m s}^{-1}$. While the current model (Eqs. 8, 16, and 17) resulted in the value of k_s of 5.16×10^{-6} , which provided a slightly lower value but in the same level of order.

There could be a number of reasons for the discrepancies of the k_s calculated using the current model with that of using the conventional mass transfer model:

- (1) An error from the assumption of constant interface thickness (δ) during the reaction. δ can change as the reaction proceed, depending on the flow conditions in each of the liquid silicon and slag phase. Disturbance at the interface, leading to interfacial instability and emulsification of one phase to another, may also occur. This intense flow around the interface can significantly affect the δ to the point that the two films diffusion model is not applicable anymore.
- (2) The k_s value determined in the previous studies itself brings its own errors and uncertainty from its experiments and calculation procedure.
- (3) Another source of error could be from the value of $C_{[B]e}$ (concentration of B in the silicon at equilibrium) selected for the calculation in kinetics equations. While this will not affect the fitting of the concentration *vs* time, it may affect the value of calculated k_s . In the previous studies by Islam *et al.* $C_{[B]e}$ was pre-assumed from equilibrium calculations using FactSage software, *i.e.*, $C_{[B]e} = 65 \text{ ppm}$ to 15.1 mol m^{-3} for one of the case. However, the experimental data show that the boron concentration arrived at a plateau (leveled) at around 100 ppm after 2700 s, which was higher than that calculated using FactSage. Appendix IV shows a

Table VI. Results of Wang's *et al.*^[17] Kinetics Data Processing Using the Two Approaches

Kinetics Model	Equation	Parameter	Value	Unit
Conventional Mass Transfer Kinetics Model	11	k_s	5.58×10^{-6}	m s^{-1}
Current Model	8	$D_{(B)}$	9.53×10^{-9}	$\text{m}^2 \text{ s}^{-1}$
	8	$\Delta\phi_s$	0.0678	V
	15, 16	k_s	5.16×10^{-6}	m s^{-1}

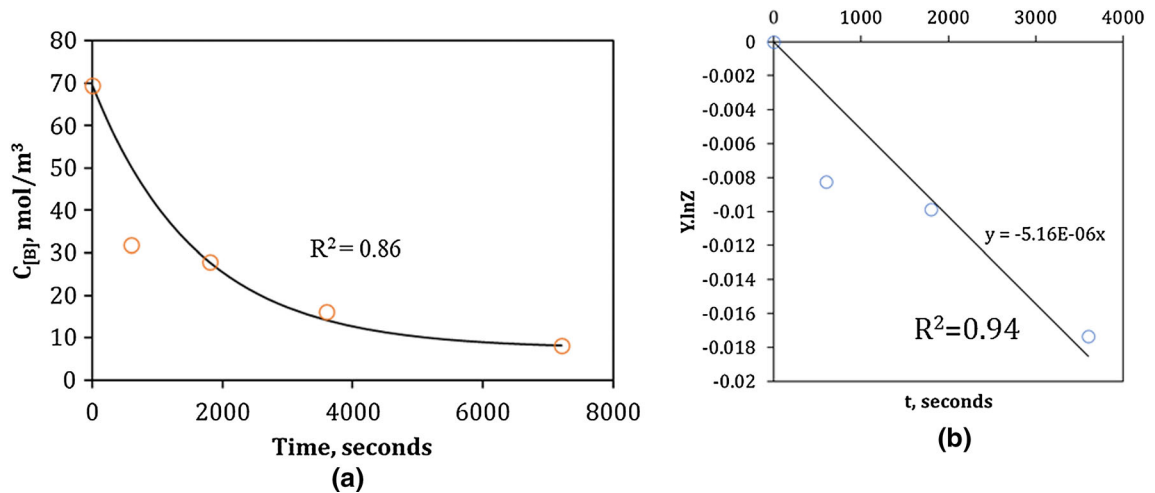


Fig. 9—(a) Kinetics data fitting of B concentration in Si with time, with 3 V applied at 1773 K, using Eq. [8], and (b) in an integrated form using Eq. [15]. Original data were from Wang *et al.*^[17]

result on calculation that show that different $C_{[B]e}$ values can affect the calculated k_s . Further checking of Eq. [16] for self-consistency (dimension/unit analysis and extremity test) is presented in Appendix V.

Overall, as can be seen from Eq. [7], there are many parameters affecting k_s . Slight changes in any of the parameter in the equation can provide variation to the results. Nevertheless, there are two major consistent trends observed from the results: (1) the addition of Al_2O_3 to the slag reduced the overall kinetics and (2) at higher voltage, the mass transfer coefficient was increasing.

The current model was developed assuming a diffusion-controlled model (with diffusion layer at the interface) which assumed that k_s is proportional to $D_{(B)}$. It is very likely that this approach is insufficient due to the reasons mentioned in Point (1). An approach based on other mass transfer models (such as surface renewal model) could be developed to improve the correlation, which will be the focus of future work by the authors.

IV. CONCLUSIONS

The analysis of kinetics of boron removal from silicon into slag through electrically enhanced refining, where external electrical potential was applied, was investigated in this study. The kinetics analysis was carried out using a kinetic model (based on the combination of Fick's first law of diffusion and Nernst–Planck equations) and built upon an approach initially utilized by Kim *et al.* that incorporate explicitly the voltage difference at the interface in the kinetic equation. The approach was modified to simultaneously solve the diffusivity of boron in the slag phase and the interfacial potential difference between the slag and the silicon. Overall, the key conclusions obtained from the current study are as follows:

- (1) The kinetic model proposed has been successfully applied and adequately described the kinetics of boron removal from silicon enhanced by external electrical potential for two sets of data, *i.e.*, from the current study (Islam *et al.*) and from Wang *et al.*
- (2) The addition of external potential difference had a positive impact on both, the rate of boron removal from silicon and the final boron concentration in silicon.
- (3) The addition of Al_2O_3 in the slag reduced the diffusivity of boron in the slag phase, as well as reduced the electrical conductivity of the slag.
- (4) The calculated potential difference across the slag phase ($\Delta\phi_s$) was generally proportional to the applied external voltage in the system ($\Delta\phi$) and on the slag phase mass transfer coefficient (k_s).
- (5) The relationship between slag-phase mass transfer coefficient (k_s) and boron diffusivity in the slag phase ($D_{(B)}$) and potential difference across the slag ($\Delta\phi_s$) was developed.
- (6) The slag phase mass transfer coefficient (k_s) calculated using the developed model was found to be slightly smaller compared to the value calculated

using a conventional mass transfer kinetics model. It appears that an approach based on other mass transfer models (such as surface renewal model) could be developed to improve the correlation.

ACKNOWLEDGMENTS

The authors gratefully acknowledge financial support from SUPRA (Swinburne University Postgraduate Research Award) scholarship; as well as from Australia Renewable Energy Agency (ARENA), Grant number 2020RND011.

COMPETING INTEREST

The authors declare that they have no known competing financial interests or personal relationships that could have appeared to influence the work reported in this paper.

AUTHOR CONTRIBUTIONS

ADPP: conceptualization, kinetics model analysis, data fitting, writing—original draft, and visualization. MSI: data collection, resources. KLA: investigation, supervision, writing—review and editing. HTBMP: supervision. GAB: supervision, writing—review and editing. MAR: investigation, supervision, writing—review and editing, project administration, and funding acquisition.

FUNDING

Open Access funding enabled and organized by CAUL and its Member Institutions.

OPEN ACCESS

This article is licensed under a Creative Commons Attribution 4.0 International License, which permits use, sharing, adaptation, distribution and reproduction in any medium or format, as long as you give appropriate credit to the original author(s) and the source, provide a link to the Creative Commons licence, and indicate if changes were made. The images or other third party material in this article are included in the article's Creative Commons licence, unless indicated otherwise in a credit line to the material. If material is not included in the article's Creative Commons licence and your intended use is not permitted by statutory regulation or exceeds the permitted use, you will need to obtain permission directly from the copyright holder. To view a copy of this licence, visit <http://creativecommons.org/licenses/by/4.0/>.

APPENDIX

EQUATION DERIVATION: FICK'S FIRST DIFFUSION LAW

Main equation:

$$-\frac{dC_{[B]}}{dt} = -k_m \frac{A}{V_{Si}} (C_{[B]} - C_{[B]}^i). \quad [A1]$$

Considering the driving force on the right-hand side of the equation:

$$(C_{[B]} - C_{[B]}^i) \quad [A2]$$

$$(C_{[B]}^i) = \frac{C_{[B]} \delta k_m + C_{(B)} D_{(B)} (1 - \frac{Fz}{RT} \frac{\delta}{L} \Delta \phi_s)}{\delta k_m + L_B^o D_{(B)} \exp(\frac{Fz}{RT} \Delta \phi_s)} \quad [A3]$$

$$(C_{[B]} - C_{[B]}^i) = \left(C_{[B]} - \frac{C_{[B]} \delta k_m + C_{(B)} D_{(B)} (1 - \frac{Fz}{RT} \frac{\delta}{L} \Delta \phi_s)}{\delta k_m + L_B^o D_{(B)} \exp(\frac{Fz}{RT} \Delta \phi_s)} \right) \quad [A4]$$

$$(C_{[B]} - C_{[B]}^i) = \left(\frac{C_{[B]} (\delta k_m + L_B^o D_{(B)} \exp(\frac{Fz}{RT} \Delta \phi_s))}{\delta k_m + L_B^o D_{(B)} \exp(\frac{Fz}{RT} \Delta \phi_s)} - \frac{C_{[B]} \delta k_m + C_{(B)} D_{(B)} (1 - \frac{Fz}{RT} \frac{\delta}{L} \Delta \phi_s)}{\delta k_m + L_B^o D_{(B)} \exp(\frac{Fz}{RT} \Delta \phi_s)} \right) \quad [A5]$$

$$(C_{[B]} - C_{[B]}^i) = \left(\frac{C_{[B]} \delta k_m + C_{[B]} L_B^o D_{(B)} \exp(\frac{Fz}{RT} \Delta \phi_s) - C_{[B]} \delta k_m - C_{(B)} D_{(B)} (1 - \frac{Fz}{RT} \frac{\delta}{L} \Delta \phi_s)}{\delta k_m + L_B^o D_{(B)} \exp(\frac{Fz}{RT} \Delta \phi_s)} \right) \quad [A6]$$

$$(C_{[B]} - C_{[B]}^i) = \left(\frac{C_{[B]} L_B^o D_{(B)} \exp(\frac{Fz}{RT} \Delta \phi_s) - C_{(B)} D_{(B)} (1 - \frac{Fz}{RT} \frac{\delta}{L} \Delta \phi_s)}{\delta k_m + L_B^o D_{(B)} \exp(\frac{Fz}{RT} \Delta \phi_s)} \right) \quad [A7]$$

From the boron mass balance:

$$C_{(B)} = (C_{[B]}^0 - C_{[B]}) \frac{V_{Si}}{V_S} \quad [A8]$$

$$(C_{[B]} - C_{[B]}^i) = \left(\frac{C_{[B]} L_B^o D_{(B)} \exp(\frac{Fz}{RT} \Delta \phi_s) - (C_{[B]}^0 - C_{[B]}) \frac{V_{Si}}{V_S} D_{(B)} (1 - \frac{Fz}{RT} \frac{\delta}{L} \Delta \phi_s)}{\delta k_m + L_B^o D_{(B)} \exp(\frac{Fz}{RT} \Delta \phi_s)} \right) \quad [A9]$$

$$(C_{[B]} - C_{[B]}^i) = \left(\frac{C_{[B]} L_B^o D_{(B)} \exp(\frac{Fz}{RT} \Delta \phi_s) + C_{[B]} \frac{V_{Si}}{V_S} D_{(B)} (1 - \frac{Fz}{RT} \frac{\delta}{L} \Delta \phi_s) - C_{[B]}^0 \frac{V_{Si}}{V_S} D_{(B)} (1 - \frac{Fz}{RT} \frac{\delta}{L} \Delta \phi_s)}{k_m + L_B^o D_{(B)} \exp(\frac{Fz}{RT} \Delta \phi_s)} \right) \quad [A10]$$

$$(C_{[B]} - C_{[B]}^i) = D_{(B)} \left(\frac{C_{[B]} \left\{ L_B^o \exp(\frac{Fz}{RT} \Delta \phi_s) + \frac{V_{Si}}{V_S} (1 - \frac{Fz}{RT} \frac{\delta}{L} \Delta \phi_s) \right\} - C_{[B]}^0 \frac{V_{Si}}{V_S} (1 - \frac{Fz}{RT} \frac{\delta}{L} \Delta \phi_s)}{\delta k_m + L_B^o D_{(B)} \exp(\frac{Fz}{RT} \Delta \phi_s)} \right) \quad [A11]$$

Substitution to main equation:

$$\frac{dC_{[B]}}{dt} = -k_m \frac{A}{V_{Si}} \frac{D_{(B)} \left(C_{[B]} \left\{ L_B^o \exp(\frac{Fz}{RT} \Delta \phi_s) + \frac{V_{Si}}{V_S} (1 - \frac{Fz}{RT} \frac{\delta}{L} \Delta \phi_s) \right\} - C_{[B]}^0 \frac{V_{Si}}{V_S} (1 - \frac{Fz}{RT} \frac{\delta}{L} \Delta \phi_s) \right)}{\delta k_m + L_B^o D_{(B)} \exp(\frac{Fz}{RT} \Delta \phi_s)} \quad [A12]$$

$$\frac{-dC_{[B]}}{C_{[B]} \left\{ L_B^o \exp(\frac{Fz}{RT} \Delta \phi_s) + \frac{V_{Si}}{V_S} (1 - \frac{Fz}{RT} \frac{\delta}{L} \Delta \phi_s) \right\} - C_{[B]}^0 \frac{V_{Si}}{V_S} (1 - \frac{Fz}{RT} \frac{\delta}{L} \Delta \phi_s)} = -k_m \frac{A}{V_{Si}} \frac{D_{(B)} dt}{\left\{ \delta k_m + L_B^o D_{(B)} \exp(\frac{Fz}{RT} \Delta \phi_s) \right\}} \quad [A13]$$

Upon integration:

$$\frac{1}{\left\{ L_B^o \exp(\frac{Fz}{RT} \Delta \phi_s) + \frac{V_{Si}}{V_S} (1 - \frac{Fz}{RT} \frac{\delta}{L} \Delta \phi_s) \right\}} \ln \frac{C_{[B]} \left\{ L_B^o \exp(\frac{Fz}{RT} \Delta \phi_s) + \frac{V_{Si}}{V_S} (1 - \frac{Fz}{RT} \frac{\delta}{L} \Delta \phi_s) \right\} - C_{[B]}^0 \frac{V_{Si}}{V_S} (1 - \frac{Fz}{RT} \frac{\delta}{L} \Delta \phi_s)}{C_{[B]}^0 \left\{ L_B^o \exp(\frac{Fz}{RT} \Delta \phi_s) + \frac{V_{Si}}{V_S} (1 - \frac{Fz}{RT} \frac{\delta}{L} \Delta \phi_s) \right\} - C_{[B]}^0 \frac{V_{Si}}{V_S} (1 - \frac{Fz}{RT} \frac{\delta}{L} \Delta \phi_s)} = -k_m \frac{A}{V_{Si}} \frac{D_{(B)} t}{\left\{ \delta k_m + L_B^o D_{(B)} \exp(\frac{Fz}{RT} \Delta \phi_s) \right\}} \quad [A14]$$

$$\ln \frac{C_{[B]} \left\{ L_B^o \exp(\frac{Fz}{RT} \Delta \phi_s) + \frac{V_{Si}}{V_S} (1 - \frac{Fz}{RT} \frac{\delta}{L} \Delta \phi_s) \right\} - C_{[B]}^0 \frac{V_{Si}}{V_S} (1 - \frac{Fz}{RT} \frac{\delta}{L} \Delta \phi_s)}{C_{[B]}^0 \left\{ L_B^o \exp(\frac{Fz}{RT} \Delta \phi_s) + \frac{V_{Si}}{V_S} (1 - \frac{Fz}{RT} \frac{\delta}{L} \Delta \phi_s) \right\} - C_{[B]}^0 \frac{V_{Si}}{V_S} (1 - \frac{Fz}{RT} \frac{\delta}{L} \Delta \phi_s)} = -k_m \frac{A}{V_{Si}} \frac{\left\{ L_B^o \exp(\frac{Fz}{RT} \Delta \phi_s) + \frac{V_{Si}}{V_S} (1 - \frac{Fz}{RT} \frac{\delta}{L} \Delta \phi_s) \right\} D_{(B)} t}{\left\{ \delta k_m + L_B^o D_{(B)} \exp(\frac{Fz}{RT} \Delta \phi_s) \right\}} \quad [A15]$$

$$\ln \frac{C_{[B]} \left\{ L_B^o \exp(\frac{Fz}{RT} \Delta \phi_s) + \frac{V_{Si}}{V_S} (1 - \frac{Fz}{RT} \frac{\delta}{L} \Delta \phi_s) \right\} - C_{[B]}^0 \frac{V_{Si}}{V_S} (1 - \frac{Fz}{RT} \frac{\delta}{L} \Delta \phi_s)}{C_{[B]}^0 \left\{ L_B^o \exp(\frac{Fz}{RT} \Delta \phi_s) \right\}} = -k_m \frac{A}{V_{Si}} \frac{\left\{ L_B^o \exp(\frac{Fz}{RT} \Delta \phi_s) + \frac{V_{Si}}{V_S} (1 - \frac{Fz}{RT} \frac{\delta}{L} \Delta \phi_s) \right\} D_{(B)} t}{\left\{ \delta k_m + L_B^o D_{(B)} \exp(\frac{Fz}{RT} \Delta \phi_s) \right\}} \quad [A16]$$

$$\frac{C_{[B]} \left\{ L_B^o \exp(\frac{Fz}{RT} \Delta \phi_s) + \frac{V_{Si}}{V_S} (1 - \frac{Fz}{RT} \frac{\delta}{L} \Delta \phi_s) \right\} - C_{[B]}^0 \frac{V_{Si}}{V_S} (1 - \frac{Fz}{RT} \frac{\delta}{L} \Delta \phi_s)}{C_{[B]}^0 \left\{ L_B^o \exp(\frac{Fz}{RT} \Delta \phi_s) \right\}} = \exp \left(-k_m \frac{A}{V_{Si}} \frac{\left\{ L_B^o \exp(\frac{Fz}{RT} \Delta \phi_s) + \frac{V_{Si}}{V_S} (1 - \frac{Fz}{RT} \frac{\delta}{L} \Delta \phi_s) \right\} D_{(B)} t}{\left\{ \delta k_m + L_B^o D_{(B)} \exp(\frac{Fz}{RT} \Delta \phi_s) \right\}} \right) \quad [A17]$$

$$C_{[B]} = \frac{C_{[B]}^0 \left\{ L_B^o \exp(\frac{Fz}{RT} \Delta \phi_s) \right\} \exp \left(-k_m \frac{A}{V_{Si}} \frac{\left\{ L_B^o \exp(\frac{Fz}{RT} \Delta \phi_s) + \frac{V_{Si}}{V_S} (1 - \frac{Fz}{RT} \frac{\delta}{L} \Delta \phi_s) \right\} D_{(B)} t}{\left\{ \delta k_m + L_B^o D_{(B)} \exp(\frac{Fz}{RT} \Delta \phi_s) \right\}} \right)}{+ C_{[B]}^0 \frac{V_{Si}}{V_S} \left(1 - \frac{Fz}{RT} \frac{\delta}{L} \Delta \phi_s \right) \left\{ L_B^o \exp(\frac{Fz}{RT} \Delta \phi_s) + \frac{V_{Si}}{V_S} \left(1 - \frac{Fz}{RT} \frac{\delta}{L} \Delta \phi_s \right) \right\}} \quad [A18]$$

LIST OF PARAMETERS AND VALUES USED IN THE EQUATIONS

See Table VII.

Table VII. List of Parameters and Values Used in the Equations

Parameter	Value	Unit	Note
M_B	10.81	g mol ⁻¹	atom mass of boron
L_B^0	0.912698413		standard boron partitioning
A	0.000103415	m ²	interface area
F	96,485	C mol ⁻¹	Faraday's constant
ρ_s	2,573.01	kg m ⁻³	35CaO-65SiO ₂
	2,670.73	kg m ⁻³	32CaO-59SiO ₂ -9Al ₂ O ₃
	2,735.03	kg m ⁻³	30CaO-55SiO ₂ -16Al ₂ O ₃
T	1,823	K	temperature
ρ_{silicon}	2,503.93	kg m ⁻³	density of silicon
m_{sil}	0.002	kg	silicon mass
V_{si}	7.98743×10^{-7}	m ³	silicon volume
m_{slag}	0.0036	kg	slag mass
V_s	1.39914×10^{-6}	m ³	slag volume
δ	0.0001	m	interface thickness
L	0.013529367	m	Slag's depth (V/A)

EQUATION DERIVATION: SLAG-CONTROLLED MASS TRANSFER KINETICS AND FICK'S FIRST LAW OF DIFFUSION

$$\frac{dC_{[B]}}{dt} = -k_m \frac{A D_{(B)}}{V_{\text{Si}}} \left(C_{[B]} \left\{ L_B^0 \exp\left(\frac{Fz}{RT} \Delta\phi_s\right) + \frac{V_{\text{Si}}}{V_s} \left(1 - \frac{Fz}{RTL} \Delta\phi_s\right) \right\} - C_{[B]}^0 \frac{V_{\text{Si}}}{V_s} \left(1 - \frac{Fz}{RTL} \Delta\phi_s\right) \right) \quad [\text{A19}]$$

$$\frac{dC_{[B]}}{dt} = -\frac{Ak_s}{V_{\text{Si}}} \left(\frac{C_{[B]_0}}{C_{[B]_e}} (C_{[B]} - C_{[B]_e}) \right) \quad [\text{A20}]$$

Equating the two equations:

$$k_m \frac{A D_{(B)}}{V_{\text{Si}}} \left(C_{[B]} \left\{ L_B^0 \exp\left(\frac{Fz}{RT} \Delta\phi_s\right) + \frac{V_{\text{Si}}}{V_s} \left(1 - \frac{Fz}{RTL} \Delta\phi_s\right) \right\} - C_{[B]}^0 \frac{V_{\text{Si}}}{V_s} \left(1 - \frac{Fz}{RTL} \Delta\phi_s\right) \right) = \frac{Ak_s}{V_{\text{Si}}} \left(\frac{C_{[B]_0}}{C_{[B]_e}} (C_{[B]} - C_{[B]_e}) \right) \quad [\text{A21}]$$

$$k_s = \frac{k_m C_{[B]_e} D_{(B)}}{C_{[B]_0} (C_{[B]} - C_{[B]_e})} \left(C_{[B]} \left\{ L_B^0 \exp\left(\frac{Fz}{RT} \Delta\phi_s\right) + \frac{V_{\text{Si}}}{V_s} \left(1 - \frac{Fz}{RTL} \Delta\phi_s\right) \right\} - C_{[B]}^0 \frac{V_{\text{Si}}}{V_s} \left(1 - \frac{Fz}{RTL} \Delta\phi_s\right) \right) \quad [\text{A22}]$$

Because the mass transfer coefficient is not affected by time, any point in the sampling data can be used. At $t = 0$, $C_{[B]} = C_{[B]_0}$.

$$k_s = \frac{k_m C_{[B]_e} D_{(B)}}{C_{[B]_0} (C_{[B]_0} - C_{[B]_e})} \left(L_B^0 \exp\left(\frac{Fz}{RT} \Delta\phi_s\right) + \frac{V_{\text{Si}}}{V_s} \left(1 - \frac{Fz}{RTL} \Delta\phi_s\right) - C_{[B]}^0 \frac{V_{\text{Si}}}{V_s} \left(1 - \frac{Fz}{RTL} \Delta\phi_s\right) \right) \quad [\text{A23}]$$

$$k_s = \frac{k_m C_{[B]_e} D_{(B)}}{C_{[B]_0} (C_{[B]_0} - C_{[B]_e})} \left(C_{[B]_0} L_B^0 \exp\left(\frac{Fz}{RT} \Delta\phi_s\right) \right) \quad [\text{A24}]$$

$$k_s = \frac{k_m C_{[B]_e} D_{(B)}}{(C_{[B]_0} - C_{[B]_e})} \left(L_B^0 \exp\left(\frac{Fz}{RT} \Delta\phi_s\right) \right) \quad [\text{A25}]$$

EFFECT OF $C_{[B]_e}$ ON THE CALCULATED k_s

Using error minimization technique, one can back calculate the value of $C_{[B]_e}$ that results in k_s with minimized difference compared to that reported by Islam *et al.* as shown in Table VIII. It was found that the resulting $C_{[B]_e}$ was 21.28 mol m⁻³ with 22 pct error average. This result shows that different values of $C_{[B]_e}$ can result in better k_s fitting.

Table VIII. Recalculated k_s with $C_{[B]_e} = 21.28 \text{ mol m}^{-3}$

Sample (Weight Percent)	$k_s, \text{ m s}^{-1}$ (From Current Model)	$k_s, \text{ m s}^{-1}$ (Reported by Islam <i>et al.</i> *)	Errors/Differences (Percent)
35CaO-65SiO ₂	2.05×10^{-6}	$*2.59 \times 10^{-6}$	26
	2.11×10^{-6}	$*3.59 \times 10^{-6}$	41
	2.15×10^{-6}	$*4.25 \times 10^{-6}$	50
32CaO-59SiO ₂ -9Al ₂ O ₃	2.03×10^{-6}	$*1.86 \times 10^{-6}$	12
	2.09×10^{-6}	$*2.36 \times 10^{-6}$	15
	2.11×10^{-6}	$*2.76 \times 10^{-6}$	24
	2.14×10^{-6}	$*3.29 \times 10^{-6}$	35
30CaO-54SiO ₂ -16Al ₂ O ₃	1.41×10^{-6}	$*1.38 \times 10^{-6}$	0
	1.85×10^{-6}	$*1.62 \times 10^{-6}$	14
	2.01×10^{-6}	$*1.86 \times 10^{-6}$	8
	2.09×10^{-6}	$*2.53 \times 10^{-6}$	17
Average			22

*Islam *et al.* [9,16,22]

DIMENSION ANALYSIS AND EXTREMITY TEST FOR CHECKING OF EQ. [16]

Dimension/unit checking for Eq. [16] was quickly carried out. The units of k_s , k_m , $C_{[B]e}$, $D_{(B)}$, F , z , R , T , $\Delta\phi_s$, and δ are $\left[\frac{m}{s}\right]$, $\left[\frac{m}{s}\right]$, $\left[\frac{mol}{m^3}\right]$, $\left[\frac{m^2}{s}\right]$, $[C \text{ mol}^{-1}]$, $[dimensionless]$, $[J \text{ mol}^{-1} \text{ K}^{-1}]$, $[K]$, $\left[\frac{J}{C}\right]$ and $[m]$ respectively. All units are equal:

$$k_s = \frac{k_m C_{[B]e} D_{(B)} (L_B^o \exp(\frac{Fz}{RT} \Delta\phi_s))}{(C_{[B]0} - C_{[B]e}) \{ \delta k_m + L_B^o D_{(B)} \exp(\frac{Fz}{RT} \Delta\phi_s) \}} \quad [A26]$$

$$\left[\frac{m}{s}\right] = \frac{\left[\frac{m}{s}\right] \left[\frac{mol}{m^3}\right] \left[\frac{m^2}{s}\right] \exp\left[\frac{C \text{ mol}^{-1} J}{J \text{ mol}^{-1} K^{-1} K}\right]}{\left[\frac{mol}{m^3}\right] \left([m] \left[\frac{m}{s}\right] + [m] \left[\frac{m}{s}\right] \exp\left[\frac{C \text{ mol}^{-1} J}{J \text{ mol}^{-1} K^{-1} K}\right] \right)} \quad [A27]$$

$$\left[\frac{m}{s}\right] = \left[\frac{m}{s}\right] \quad [A28]$$

In addition, extremity test can be carried out for zero value of the interface thickness (δ). At this point, there are no gradients of boron concentration at the interface. This also means that the reaction is no longer controlled in the slag phase. Mathematically, this is represented by constant value of k_s as shown in Equation below. In this equation, the values of $D_{(B)}$ and $\Delta\Phi_{\text{int}}$ are no longer affecting the k_s , which is in a good agreement with the previous explanation.

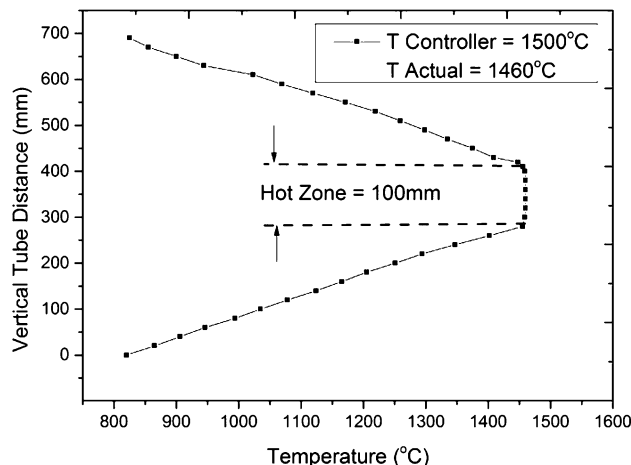


Fig. A1—Temperature profile of the tube furnace at 1773 K (1500 °C).

$$k_s = \frac{k_m C_{[B]e}}{(C_{[B]0} - C_{[B]e})} \quad [A29]$$

TUBE FURNACE TEMPERATURE PROFILE

The temperature profile measurement of the vertical tube furnace that was used in the experiment is presented in Figure A1.

REFERENCES

1. U.S. Department of Energy: *Energy Effic. Renew. Energy*.
2. P. Bojek and H. Bahar: Solar PV, <https://www.iea.org/reports/solar-pv>. Accessed 2 Mar 2022.
3. V. Fiandra, L. Sannino, C. Andreozzi, and G. Graditi: *Waste Manag.*, 2019, vol. 84, pp. 91–101.
4. M.S. Chowdhury, K.S. Rahman, T. Chowdhury, N. Nuthammachot, K. Techato, M. Akhtaruzzaman, S.K. Tiong, K. Sopian, and N. Amin: *Energy Strateg. Rev.*, 2020, vol. 27, p. 100431.
5. M.D. Johnston, L.T. Khajavi, M. Li, S. Sokhanvaran, and M. Barati: *Jom*, 2012, vol. 64, pp. 935–45.
6. L.T. Khajavi and M. Barati: *High Temp. Mater. Process.*, 2012, vol. 31, pp. 627–31.
7. N. Yuge, M. Abe, K. Hanazawa, H. Baba, N. Nakamura, Y. Kato, Y. Sakaguchi, S. Hiwasa, and F. Aratani: *Prog. Photovoltaics Res. Appl.*, 2001, vol. 9, pp. 203–09.
8. O. Espen and S. Rolseth: *Metall. Mater. Trans. B Process Metall. Mater. Process. Sci.*, 2010, vol. 41, pp. 295–302.
9. M.S. Islam and M.A. Rhamdhani: *Metall. Mater. Trans. B Process Metall. Mater. Process. Sci.*, 2018, vol. 49, pp. 3171–185.
10. S. Thomas, M. Barati, and K. Morita: *JOM J. Miner. Met. Mater. Soc.*, 2021, vol. 73, pp. 282–92.
11. M.S. Islam, M.A. Rhamdhani, and G.A. Brooks: *Metall. Mater. Trans. B Process Metall. Mater. Process. Sci.*, 2013, vol. 45, pp. 1–5.
12. W.D. Judge, J. Paeng, and G. Azimi: *Electrochim. Acta*, 2021, vol. 389, p. 138755.
13. W.D. Judge, J. Paeng, and G. Azimi: *Electrochim. Acta*, 2022, vol. 406, p. 139801.
14. S.H. Lee and D.J. Min: *Sep. Purif. Technol.*, 2020, <https://doi.org/10.1016/j.seppur.2019.116231>.
15. D.H. Kim and Y.B. Kang: *Metall. Mater. Trans. B Process Metall. Mater. Process. Sci.*, 2021, vol. 52, pp. 2960–970.
16. M.S. Islam, M.A. Rhamdhani, and G.A. Brooks: in *TMS Annual Meeting*, 2014, pp. 587–95.
17. Z. Wang, Z. Ge, J. Liu, G. Qian, and B. Du: *Sep. Purif. Technol.*, 2018, vol. 199, pp. 134–39.
18. D.H. Kim, W. Kim, and Y.B. Kang: *Metall. Mater. Trans. B Process Metall. Mater. Process. Sci.*, 2018, vol. 49, pp. 1311–321.
19. D.-H. Kim, W. Kim, and Y.-B. Kang: *J. Electrochem. Soc.*, 2018, vol. 165, pp. E816–825.
20. Y.N. Toulouevski and I.Y. Zinurov: *Innovation in Electric Arc Furnaces*, Springer, Berlin, 2010.
21. S.H. Lee and D.J. Min: *Materials (Basel)*, 2020, <https://doi.org/10.3390/ma13112478>.
22. M.S. Islam: Swinburne University of Technology, 2015.
23. A. Paul, T. Laurila, V. Vuorinen, and S.V. Divinski: *Thermodynamics, Diffusion and the Kirkendall Effect in Solids*, vol. 9783319074, Springer, Cham, 2014.
24. R. Maex: *J. Integr. Neurosci.*, 2017, vol. 16, pp. 73–91.
25. L. Muhmood and S. Seetharaman: *Metall. Mater. Trans. B Process Metall. Mater. Process. Sci.*, 2010, vol. 41, pp. 833–40.
26. R.K. Endo, Y. Fujihara, and M. Susa: Tokyo Institute of Technology, 2003.
27. H. Chen, K. Morita, X. Ma, Z. Chen, and Y. Wang: *Sol. Energy Mater. Sol. Cells*, 2019, vol. 203, p. 110169.

28. E. Krystad, L.K. Jakobsson, K. Tang, and G. Tranell: *Metall. Mater. Trans. B Process Metall. Mater. Process. Sci.*, 2017, vol. 48, pp. 2574–582.
29. J. Zhang, Z. Liu, J. Zhang, C. Wang, H. Ma, H. Li, and J. Fan: *Preprints*, <https://doi.org/10.20944/preprints202109.0172.v1>.
30. H. Yu, J. Xu, J. Zhang, and X. Wang: *Ironmak. Steelmak.*, 2016, vol. 43, pp. 607–15.
31. R.S.E. Schneider, M. Molnar, G. Klösch, and C. Schüller: *Metall. Mater. Trans. B Process Metall. Mater. Process. Sci.*, 2020, vol. 51, pp. 1904–911.
32. Z. Wang, Y. Sun, S. Sridhar, M. Zhang, M. Guo, and Z. Zhang: *Metall. Mater. Trans. B Process. Metall. Mater. Process. Sci.*, 2015, vol. 46, pp. 537–41.
33. L. Segers, A. Fontana, and R. Winand: *Can. Metall. Q.*, 1983, vol. 22, pp. 429–35.
34. G.-H. Zhang, J.-H. Liu, and K.-C. Chou: in *Proceedings of The 10th International Conference on Molten Slags, Fluxes and Salts (MOLTEN16)*, Springer, 2016, pp. 1335–41.
35. H. Nishimoto, Y. Kang, T. Yoshikawa, and K. Morita: *High Temp. Mater. Process.*, 2012, vol. 31, pp. 471–77.

Publisher's Note Springer Nature remains neutral with regard to jurisdictional claims in published maps and institutional affiliations.